

1 **Interpretation of Multi-scale Permeability Data through an Information Theory Perspective**

2 **Aronne Dell’Oca, Alberto Guadagnini, and Monica Riva**

3 Department of Civil and Environmental Engineering, Politecnico di Milano, 20133, Milano, Italy;

4 Corresponding author: Aronne Dell’Oca (aronne.delloc@polimi.it)

5
6 **Key Points**

- 7 • Information Theory allows characterizing information content of permeability data related to
8 differing measurement scales.
- 9 • An increase of the measurement scale is associated with quantifiable loss of information about
10 permeability.
- 11 • Redundant, unique and synergetic contributions of information are evaluated for triplets of
12 permeability datasets, each taken at a given scale.

Abstract

We employ elements of Information Theory to quantify (i) the information content related to data collected at given measurement scales within the same porous medium domain, and (ii) the relationships among Information contents of datasets associated with differing scales. We focus on gas permeability data collected over a Berea Sandstone and a Topopah Spring Tuff blocks, considering four measurement scales. We quantify the way information is shared across these scales through (i) the Shannon entropy of the data associated with each support scale, (ii) mutual information shared between data taken at increasing support scales, and (iii) multivariate mutual information shared within triplets of datasets, each associated with a given scale. We also assess the level of uniqueness, redundancy and synergy (rendering, i.e., information partitioning) of information content that the data associated with the intermediate and largest scales provide with respect to the information embedded in the data collected at the smallest support scale in a triplet.

Plain Language Summary

Characterization of the permeability of a geophysical system, or part of it, is a key aspect in many environmental settings. Permeability of natural systems typically exhibits spatial variations and its spatially heterogeneous pattern is linked with the size of observation/measurement/support scale. As the latter becomes coarser, the system appearance is less heterogeneous. As such, sets of permeability data associated with differing support scales provide diverse amounts of information. In this contribution, we leverage on elements of Information Theory to quantify the information content of gas permeability datasets collected over a Berea Sandstone and a Topopah Spring Tuff blocks and associated with four measurement scales. We then characterize the nature of the information shared by the diverse datasets, in terms of redundant, unique and synergetic forms of information.

1. Introduction

Characterization of permeability of porous media plays a major role in a variety of hydrological settings. There are abundant studies documenting that permeability values and their associated statistics depend on a variety of scales, i.e., the measurement support (or data support), the sampling window (domain of investigation), the spatial correlation (degree of structural coherence) and the spatial resolution (rendering the degree of the descriptive detail associated with the characterization of a porous system) (see e.g., Brace 1984; Clauser, 1992; Neuman, 1994; Schad and Teutsch, 1994; Rovey and Cherkauer, 1995; Sanchez-Villa et al., 1996; Schulze-Makuch and Cherkauer, 1998; Schulze-Makuch et al., 1999; Tidwell and Wilson, 1999a, b, 2000; Vesselinov et al., 2001a, b; Winter and Tartakovsky, 2001; Hyun et al., 2002; Neuman and Di Federico, 2003; Maréchal et al., 2004; Illman, 2004; Cintoli et al., 2005; Riva et al., 2013; Guadagnini et al., 2013, 2018 and references therein). Among these scales, we focus here on the characteristic length associated with data collection (i.e., support scale).

In this context, experimental evidences at the laboratory scale (observation scale of the order 0.1-1.0 m) suggest that the mean value and the correlation length of the permeability field tend to increase with the size of the data support, the opposite trend being documented for the variance (e.g., Tidwell and Wilson, 1999a, 1b, 2000). Similar observations, albeit with some discrepancies, are also tied to investigations at larger scales (i.e., 10-1000 m) (Andersson et al., 1988; Guzman et al., 1994, 1996; Neumann, 1994; Schulze-Makuch and Cherkauer, 1998; Zlotnik et al., 2000; Bulter and Healey, 1998a,b). We consider here laboratory scale permeability datasets which are associated with various measurement scales.

58 The above mentioned documented pattern suggests that the spatial distribution of permeability
59 tends to be characterized by an increased degree of homogeneity (as evidenced by a decreased
60 variance and an increased spatial correlation) as the support/measurement scale increases. At the same
61 time, increasing the measurement scale somehow hampers the ability to detect locally low
62 permeability values, as reflected by the observed increased mean value of the data. As an example of
63 the kind of data we consider in this study to clearly document these features, Figure 1 depicts the
64 spatial distribution of the natural logarithm of (normalized) gas permeabilities, i.e., $Y_{r_i} = \ln(k_{r_i} / \bar{k}_{r_i})$
65 (where k_{r_i} is gas permeability and \bar{k}_{r_i} is the mean value of the data), collected across two faces of a
66 laboratory scale block of (i) a Berea Sandstone (Tidwell and Wilson, 1999a) and (ii) a Topopah Spring
67 Tuff (Tidwell and Wilson, 1999b) at four support scales r_i (see Section 2 for a detailed description).
68 As a preliminary observation, one can note that increasing the measurement scale r_i yields a
69 decreased level of descriptive detail of the heterogeneous spatial distribution of the system properties.
70 It is important to note that a reduced level of details in the description of the system properties (e.g.,
71 Y_{r_i}) could hinder reliability and accuracy of further predictions of system behavior (in terms of, e.g.,
72 flow and solute transport patterns). It is therefore relevant to quantify the amount of loss (or of
73 preservation) of the information about the system properties associated with a fine scale(s) of
74 reference as the data support increases.

75 Our study aims at providing an assessment and a firm quantification of these aspects upon
76 relying on Information Theory (IT) (e.g., Stone, 2015) and the multiscale collection of data described
77 above. We consider such a framework of analysis as it provides the elements to quantify (i) the
78 information content associated with a dataset collected at a given scale as well as (ii) the information
79 shared between pairs or triplets of data, each associated with a unique scale (while preserving the
80 design of the measurement device). In this context, IT represents a convenient theoretical framework
81 to properly assist the characterization of the way the information content is distributed across sets of
82 measurements, without being confined to a linear analysis (relying, e.g., on analyses of linear
83 correlation coefficients) or invoking some tailored assumption(s) about the nature of the
84 heterogeneity of permeability (e.g., the characterization of the datasets through a Gaussian model).

85 To the best of our knowledge, as compared to surface hydrology systems only a limited set of
86 works consider relying on IT concepts to analyze scenarios related to processes taking place in
87 subsurface porous media. Nevertheless, we note a great variety in the topics covered in these works,
88 reflecting the broad potential for applicability of IT concepts. These studies include, e.g., the works
89 of Woodbury and Ulrych (1993, 1996, 2000) who apply the principle of minimum relative entropy
90 to tackle uncertainty propagation and inverse modeling in a groundwater system. The principle of
91 maximum entropy is employed by Gotovac et al. (2010) to characterize the probability distribution
92 function of travel time of a solute migrating across a heterogeneous porous formation. Within the
93 same context, Kitanidis (1994) leverages on the definition of entropy and introduces the concept of
94 dilution index to quantify the dilution state of a solute cloud migrating within an aquifer. Mishra et
95 al. (2009) and Zeng et al. (2012) evaluate the mutual information shared between pairs of (uncertain)
96 model input(s) and output(s) of interest, and view this metric as a measure of global sensitivity.
97 Nowak and Guthke (2016) focus on sorption of metals onto soil and the identification of an optimal
98 experimental design procedure in the presence of multiple models to describe sorption. Boso and
99 Tartakovsky (2018) illustrate an IT approach to upscale/downscale equations of flow in synthetic
100 settings mimicking heterogeneous porous media. Relying on IT metrics, Butera et al. (2018) assess
101 the relevance of non-linear effects for the characterization of the spatial dependence of flow and solute

102 transport related observables. Bianchi and Pedretti (2017, 2018) developed novel concepts, mutated
103 by IT, for the characterization of heterogeneity within a porous system and its links to salient solute
104 transport features. Wellman and Regenaur-Lieb (2012) and Wellman (2013) leverage on IT concepts
105 to quantify uncertainty, and its reduction, about the spatial arrangement of geological units of a
106 subsurface formation. Recently, Mälicke et al. (2019) combine geostatistic and IT to analyze soil
107 moisture data (representative of a given measurement scale) to assess the persistence over time of the
108 spatial organization the soil moisture, under diverse hydrological regimes.

109 Here, we focus on the aforementioned datasets of Tidwell and Wilson (1999a, b) who conducted
110 extensive measurement campaigns collecting air permeability data across the faces of a Berea
111 Sandstone and a Topopah Spring Tuff blocks, considering four different support/measurement scales
112 (see Section 2 for details). While our study does not tackle directly issues associated with the way
113 one can upscale (flow or transport) attributes of porous media, we leverage on such a unique and truly
114 multiscale datasets to address research questions such as “How much information about the natural
115 logarithm of (normalized) gas permeabilities is lost as the support scale increases?” and “How
116 informative are data taken at a coarser support scale(s) with respect to those associated with a finer
117 support scale?” (see Section 3). In this sense, our study yields a unique perspective of the assessment
118 of the value of hydrogeological information collected at differing scales.

119 2. Dataset

120 We consider the datasets provided by Tidwell and Wilson (1999a, b), who rely on a
121 multisupport permeameter (MSP) to evaluate spatial distributions of air permeabilities across the
122 faces of a cubic block of Berea Sandstone (hereafter denoted as Berea) and Topopah Spring Tuff
123 (hereafter denoted as Topopah). Data are collected at uniform intervals with spacing $\Delta = 0.85$ cm
124 across a grid of 24×24 and 36×36 nodes along each face (of uniform side equal to 19.5 cm and
125 29.75 cm, to avoid boundary effects) of the Berea and the Topopah blocks, respectively. Four
126 measurement campaigns are conducted, each characterized by the use of a MSP with a tip-seal of
127 inner radius r_i ($i = 1, 2, 3, 4$) = (0.15, 0.31, 0.63, 1.27) cm and outer radius $2r_i$ (interested readers can
128 find additional details about the MSP design and functioning in Tidwell and Wilson, 1997). While
129 the precise nature and size of the support/measurement scale associated with a MSP is still under
130 study for heterogeneous media (e.g., Goggin et al., 1988; Molz et al., 2003; Tartakovsky et al., 2000),
131 hereafter we denote data associated with a given support/measurement scale by referring these to the
132 associated value of r_i . The ensuing dataset is then composed by 3456 and 6480 data points for each
133 measurement scale, r_i , for the Berea and the Topopah block, respectively (we exclude data for one
134 of the faces of the Topopah block, due to some anomalies with respect to the other faces). We consider
135 here the quantity $Y_{r_i} = \ln(k_{r_i} / \bar{k}_{r_i})$, i.e., the natural logarithm of the air permeability normalized by the
136 mean value (i.e., \bar{k}_{r_i}) of the data of the corresponding sample.

137 The two types of rocks analyzed display distinct features. The Berea sample may be classified
138 as a very fine-grained, well-sorted quartz sandstone. Following Tidwell and Wilson (1999a), visual
139 inspection of the spatial distributions of Y_{r_i} (see, e.g., Figure 1) shows that the Berea sample exhibits
140 a generally uniform spatial organization of permeabilities, devoid of particular features, with the
141 exception of a mild stratification, thus allowing to consider this sample as a fairly homogenous
142 system. Otherwise, the Topopah rock sample clearly exhibits a heterogenous structure whereas
143 pumice fragments ($\sim 23\%$ of the sample) are embedded in the surrounding matrix (see Figure 1). In

144 general, the pumice is characterized by higher permeability values than the surrounding matrix. As
145 such, the Topopah sample can be considered as a fairly heterogenous system, with a tendency to
146 display a bimodal distribution of permeability values (see also Section 4.2). In this sense, the two
147 rock samples analyzed provide two clearly distinct scenarios for the analysis of the interplay of the
148 information contained in datasets collected at diverse measurement scales.

149 We note that the IT elements described in Section 3 refer to discrete variables. While
150 corresponding definitions are available also for continuous variables (i.e., summation(s) and
151 probability mass function(s) are replaced by integral(s) and probability density function(s),
152 respectively), these are characterized by a less intuitive and immediate interpretation (e.g., Entropy
153 could be negative, infinite or could not be evaluated in case of probability density function(s)
154 involving a Dirac's delta; see, e.g., Kaiser and Schreiber, 2002; Cover and Thomas, 2006). Moreover,
155 in case the probability density functions of the analyzed continuous variables cannot be associated
156 with an analytical expression, it is necessary to subject these variables to quantization and the IT
157 metrics related to the continuous variables are estimated through their quantized counterparts (see
158 Cover and Thomas, 2006). In general, the quality of these estimates increases (in a way which
159 depends on the specific metric) with the level of quantization of the continuous variables (see, e.g.,
160 Kaiser and Schreiber, 2002). This leads us to treat Y_{r_i} as a discrete variable, a modeling choice which
161 is consistent with several previous studies (see, e.g., Ruddell and Kumar, 2009; Goodwell et al., 2017;
162 Nearing et al., 2018 and references therein).

163 3. Methodology

164 3.1 Information Theory

165 Considering a discrete random variable, X , one can quantify the associated uncertainty through
166 the Shannon entropy

$$167 \quad H(X) = \sum_{i=1}^N p_i \log_2(p_i^{-1}) \quad (1)$$

168 where N is the number of bins used to analyze the outcomes of X ; and p_i is the probability mass
169 function and $\ln(p_i^{-1})$ is the (so-called) Information (or degree of surprise) associated with the i -th
170 bin (see, e.g., Shannon, 1948). We employ base two logarithms in (1), thus leading to *bits* as unit of
171 measure for entropy and for the IT metrics we describe in the following. While other choices (relying,
172 e.g., on the natural logarithm) are admissible, the nature and meaning of the metrics we illustrate
173 remain unaffected. The Shannon entropy can be interpreted as a measure of the uncertainty associated
174 with X , i.e., $H(X)$ is largest and equal to $\log_2(N)$ in case p_i is uniform across all bins (i.e., $p_i = 1/N$
175), while it is zero when outcomes of X reside only within a single bin. Moreover, one can note that
176 Shannon entropy in (1) is directly linked to the average number of binary questions (i.e., questions
177 with a *yes* or *no* answer) one needs to ask to infer the state in which X is. In our study, samples drawn
178 from the population of the random variable X are identified with values Y_{r_i} and Shannon entropy can
179 also be interpreted as a measure of the degree of heterogeneity of the system. In this sense, considering
180 a support scale r_i , if the collected data (which are spatially distributed over the system) would cluster
181 into one (or only a few) bin(s), one could interpret the system as homogeneous (or nearly
182 homogeneous) at such a scale.

183 The information content shared by two random variables, i.e., X_1 and X_2 , is termed bivariate
 184 mutual information and is defined as

$$185 \quad I(X_1; X_2) = \sum_{i=1}^N \sum_{j=1}^M p_{i,j} \ln \left(\frac{p_{i,j}}{p_i p_j} \right) \quad (2)$$

186 where N and M represent the number of bins associated with X_1 and X_2 , respectively; p_i and p_j
 187 are marginal probability mass functions associated with X_1 and X_2 , respectively; and $p_{i,j}$ is the joint
 188 probability mass function of X_1 and X_2 . The bivariate mutual information measures the average
 189 reduction in the uncertainty (as quantified through the Shannon entropy) about one random variable
 190 that one can obtain by knowledge on the other variable (Gong et al., 2013 and references therein). As
 191 such, the bivariate mutual information (a) vanishes for two independent variables and (b) coincides
 192 with the entropy of either of the two variables when one variable fully explains the other one, i.e.,
 193 $H(X_2) = H(X_1) = I(X_1; X_2)$. In light of the latter observations, it is clear that the bivariate mutual
 194 information can be also interpreted as a measure of the degree of dependence between X_1 and X_2 .

195 When considering three discrete random variables, it is possible to quantify the amount of
 196 information that two of these (termed as sources, i.e., X_{S_1} and X_{S_2}) share with the third one (termed
 197 as target variable, i.e., X_T) upon evaluating the following multivariate mutual information

$$198 \quad I(X_{S_1}, X_{S_2}; X_T) = \sum_{i=1}^N \sum_{j=1}^M \sum_{k=1}^W p_{i,j,k} \ln \left(\frac{p_{i,j,k}}{p_{i,j} p_k} \right) \quad (3)$$

199 Here, N , M , and W represent the number of bins associated with X_{S_1} , X_{S_2} and X_T , respectively;
 200 p_k is the probability mass function of X_T ; $p_{i,j}$ is the joint probability mass function of X_{S_1} and X_{S_2}
 201 ; and $p_{i,j,k}$ is the joint probability mass function of X_{S_1} , X_{S_2} , and X_T . Relying on the partial
 202 information decomposition or information partitioning (Williams and Beer, 2010;), the multivariate
 203 mutual information in (3) can be partitioned into unique, redundant, and synergetic contributions, i.e.,

$$204 \quad I(X_{S_1}, X_{S_2}; X_T) = U(X_{S_1}; X_T) + U(X_{S_2}; X_T) + R(X_{S_1}, X_{S_2}; X_T) + S(X_{S_1}, X_{S_2}; X_T) \quad (4)$$

205 Here, $U(X_{S_1}; X_T)$ and $U(X_{S_2}; X_T)$ represent the amount of information that is uniquely provided to
 206 the target X_T by X_{S_1} and X_{S_2} , respectively (i.e., the information $U(X_{S_1}; X_T)$ cannot be provided to
 207 X_T by knowledge on X_{S_2} , a corresponding observation holding for $U(X_{S_2}; X_T)$); the redundant
 208 contribution $R(X_{S_1}, X_{S_2}; X_T)$ is the information that both source variables provide to the target (i.e.,
 209 it is the amount of information transferable to X_T that is contained in both X_{S_1} and X_{S_2}); and the
 210 synergetic contribution $S(X_{S_1}, X_{S_2}; X_T)$ is the information about X_T that knowledge on X_{S_1} and X_{S_2}
 211 brings in a synergic way. Note that the latter contribution corresponds to the amount of information
 212 that (possibly) emerges by simultaneous knowledge of the two sources and through an analysis of
 213 their joint relationship with X_T , i.e., it would not appear by knowing both X_{S_1} and X_{S_2} while
 214 analyzing their individual relationship with X_T separately. All components in (4) are positive
 215 (Williams and Beer, 2010). Figure 2 provides a graphical depiction in terms of Venn diagrams of the
 216 above information components in a system characterized by two sources and a target variable.

217 The bivariate mutual information shared by the target and each source can be written as

$$\begin{aligned}
 218 \quad I(X_{S_1}; X_T) &= U(X_{S_1}; X_T) + R(X_{S_1}, X_{S_2}; X_T) \\
 I(X_{S_2}; X_T) &= U(X_{S_2}; X_T) + R(X_{S_1}, X_{S_2}; X_T)
 \end{aligned} \tag{5}$$

219 Note that (5) reflects the nature of the information that is shared by the target and each of the sources,
 220 when these are taken separately, i.e., no synergy can be detected here. We also remark that one should
 221 expect the emergence of some redundancy of information when the two sources are correlated.

222 An additional element of relevance for the aim of our study is the interaction information

$$\begin{aligned}
 223 \quad I(X_{S_1}; X_{S_2}; X_T) &= I(X_{S_1}; X_T | X_{S_2}) - I(X_{S_1}; X_T) = \\
 &= I(X_{S_2}; X_T | X_{S_1}) - I(X_{S_2}; X_T)
 \end{aligned} \tag{6}$$

224 Here, $I(X_{S_i}; X_T | X_{S_j})$ is the bivariate mutual information shared by source X_{S_i} ($i = 1, 2$) and the
 225 target, conditional to the knowledge of source X_{S_j} ($j = 2, 1$). Note that $I(X_{S_i}; X_T | X_{S_j})$ can be
 226 evaluated in a way similar to (2) upon relying on the conditional probability for X_T . Williams and
 227 Beer (2011) show that

$$228 \quad I(X_{S_1}; X_{S_2}; X_T) = S(X_{S_1}, X_{S_2}; X_T) - R(X_{S_1}, X_{S_2}; X_T) \tag{7}$$

229 According to (7), the bivariate interaction information could be either positive, i.e., when synergetic
 230 interactions prevail over redundant contribution, or negative, i.e., when the degree of redundancy
 231 overcomes the synergetic effects.

232 Inspection of (4)-(7) reveals that an additional equation is required to evaluate all components
 233 in (4). Various strategies have been proposed in this context (e.g., Williams and Beer, 2010; Harder
 234 et al., 2013; Bertschinger et al., 2014; Griffith and Koch, 2014; Olbrich et al., 2015; Griffith and Ho,
 235 2015). We rest here on the recent partitioning strategy formalized by Goodwell and Kumar (2017),
 236 due to its capability of accounting for the (possible) dependences between sources when evaluating
 237 the unique and redundant contributions. The rationale underpinning this strategy is that (i) each of the
 238 two sources can provide a unique contribution of information to the target even as these are correlated,
 239 and (ii) redundancy should be lowest in case of independent sources. The redundant contribution can
 240 then be evaluated as (Goodwell and Kumar, 2017)

$$241 \quad R(X_{S_1}, X_{S_2}; X_T) = R_{\min}(X_{S_1}, X_{S_2}; X_T) + I_s (R_{MMI}(X_{S_1}, X_{S_2}; X_T) - R_{\min}(X_{S_1}, X_{S_2}; X_T)) \tag{8a}$$

242 with

$$\begin{aligned}
 R_{\min}(X_{S_1}, X_{S_2}; X_T) &= \max(0, -I(X_{S_1}; X_{S_2}; X_T)); \\
 R_{MMI}(X_{S_1}, X_{S_2}; X_T) &= \min(I(X_{S_2}; X_T), I(X_{S_1}; X_T)); \\
 I_s &= \frac{I(X_{S_1}; X_{S_2})}{\min(H(X_{S_1}), H(X_{S_2}))};
 \end{aligned} \tag{8b}$$

244 Goodwell and Kumar (2017) termed (8) as a rescaled measure of redundancy whereas (a)
 245 $R_{\min}(X_{S_1}, X_{S_2}; X_T)$ represents the lowest bound for redundancy, which is set on the basis of the
 246 rationale that the minimum value of redundancy must at least be equal to $-I(X_{S_1}; X_{S_2}; X_T)$ in case
 247 $I(X_{S_1}; X_{S_2}; X_T) < 0$ (thus also ensuring positiveness of the synergy; see (7)); (b) $R_{MMI}(X_{S_1}, X_{S_2}; X_T)$

248 is an upper bound, consistent with the rationale that all information from the weakest source is
 249 redundant; and (c) I_s accounts for the degree of dependence between the sources, i.e., $I_s = 0$ and
 250 $R(X_{s_1}, X_{s_2}; X_T) = R_{\min}(X_{s_1}, X_{s_2}; X_T)$ for independent sources, while $I_s = 1$ and redundancy in (8)
 251 attains its upper limit value, $R_{MMI}(X_{s_1}, X_{s_2}; X_T)$, in case of a *complete* dependency (i.e.,
 252 $X_{s_1} = f(X_{s_2})$ or vice versa) between the sources. Once the redundancy has been evaluated, all of the
 253 other components in (4) can be determined.

254 We emphasize that, despite some additional complexities, analyzing the partitioning of the
 255 multivariate mutual information provides valuable insights on the way information is shared across
 256 three variables, these being here permeability data associated with three diverse support scales. In
 257 summary, addressing information partitioning enables us to (i) quantify and (ii) characterize the
 258 nature of the information that two variables (sources) provide to a third one (target) as a *whole*, i.e.,
 259 considering the entire triplet. Doing so overcomes the limitation of depicting the system as a simple
 260 *sum of parts*, as based on solely inspecting the corresponding pairwise bivariate mutual information,
 261 which allows quantifying just the amount of information that pairs of variables (i.e., the first source
 262 and the target; and the second source and the target) share (without being able to define redundant or
 263 unique contributions, see Eq. (9)). In the context of our work, this implies that information
 264 partitioning enables us to characterize the nature of the information that permeability data collected
 265 at two support scales provide to /share with permeability data taken at a third one.

266 3.2 Implementation Aspects

267 Evaluation of the quantities introduced in Section 3.1 is accomplished according to three main
 268 steps. We employ the Kernel Density Estimator (KDE) routines in Matlab2018© to estimate the
 269 continuous counterparts of the probability mass functions p_i , p_j , $p_{i,j}$, and $p_{i,j,k}$ and assess the
 270 associated probability density functions, i.e., *pdfs*. This step enables us to smooth and regularize the
 271 available finite datasets. We then discretize the ensuing *pdfs* to evaluate the associated probability
 272 mass functions. Note that this two-step procedure allows us to obtain results that are more stable (with
 273 respect to the number of bins employed) than those that one could obtain upon discretizing directly
 274 the available finite datasets. As a final step, we evaluate the metrics detailed in Section 3 by treating
 275 separately the multi-scale measurements on each face and then averaging the ensuing face-related
 276 results for each of the two rock samples. The benefit of resting on this approach is especially critical
 277 when considering the Topopah rock, whereas pooling the data of all faces as a unique sample hindered
 278 the emergence of the bimodal behavior (i.e., the permeability values corresponding to the peaks of
 279 the bimodal distributions are slightly different depending on the face considered and the joint
 280 treatment of the data from all faces yielded a nearly unimodal distribution). We employ a binning
 281 scheme corresponding to a uniform discretization of the range delimited by the lowest and largest
 282 values detected considering all datasets associated with both rocks (i.e., we employ the same specific
 283 binning for the Berea and the Topopah rock samples to assist quantitative comparison of the results).
 284 We observe that within an IT approach the selection of a bin size is an a priori choice (see, e.g., Gong
 285 et al., 2014; Loritz et al., 2018) the influence of which should be properly assessed (see Section 4 and
 286 Supplementary Material). We inspect how the IT metrics described in Section 2 vary as a function
 287 of (i) the number of bins (i.e., we consider a number of 50, 75, 100, and 125 bins for the discretization
 288 of the range of data variability) and (ii) the size of the kernel bandwidth (which is varied within the
 289 range 0.1 - 0.4) employed in the KDE routine (see Supplementary Material, Figures SM1-3, for
 290 additional details). This analysis highlights a weak dependence of the values of the investigate IT
 291 metrics on the number of bins and on the size of the bandwidth employed in the Kernel Density

292 Estimator (KDE) procedure, the overall patterns of these metrics remaining substantially unaffected.
293 This leads us to use 100 bins and a kernel bandwidth equal to 0.3. Note that we consistently employ
294 this binning for the evaluation of all metrics introduced in Section 2.

295 We remark that the bivariate and multivariate mutual information metrics are evaluated by
296 focusing on the joint probability mass function grounded on the multi-scale data collected at the same
297 location on the sampling grids.

298 4. Results

299 Figure 3 depicts the probability mass function $p(Y_{r_i})$ for $i = 1$ (r_1 ; black symbols), 2 (r_2 ; red
300 symbols), 3 (r_3 ; blue symbols), and 4 (r_4 ; green symbols) for the (a) Berea and (b) the Topopah rock
301 samples. For both rocks the $p(Y_{r_i})$ associated with only one face is depicted (similar patterns are
302 noted for all of the remaining faces). Figure 3c depicts the Shannon entropy $H(Y_{r_i})$ as a function of
303 the MSP support scale r_i for the Berea (diamonds) and the Topopah (circles) samples. Figure 3d
304 depicts the bivariate mutual information between data collected at two distinct support scales. This
305 metric is normalized by the entropy of the data associated with the smaller support scale, i.e.,
306 $I^*(Y_{r_i}; Y_{r_j}) = I(Y_{r_i}; Y_{r_j}) / H(Y_{r_i})$ with $j > i$, for $i = 1$ (blue diamonds) and 2 (green diamonds), results for
307 the Berea (diamonds) and the Topopah (circles) samples are reported.

308 Inspection of Figure 3a-b reveals that distributions related to increasing values of r_i tend not to
309 encompass extreme values (in particular the low ones) of Y . This observation supports the fact that
310 increasing r_i favors a homogenization of the permeability values and suggests that the response of
311 the MSP tends to be only weakly sensitive to the less permeable portions of the rock that are
312 encompassed within a given measurement scale. As a consequence, the $p(Y_{r_i})$ associated with
313 increasing r_i are characterized by a reduced number of populated bins, this feature being in turn
314 reflected in the observed reduction of $H(Y_{r_i})$ with increasing r_i (Figure 3c) for both rock samples.
315 This result can be interpreted as a signature (see also the discussion about (1) in Section 3.1) of the
316 effect of increasing r_i , which yields a decrease of (i) the uncertainty about the spatial distribution of
317 the values of Y_{r_i} and (ii) the ability of capturing the degree of spatial heterogeneity of Y . Note that
318 Figure 3c suggests that the value of $H(Y_{r_i})$, given r_i , associated with the Topopah sample is always
319 higher than its counterpart associated with the Berea rock. This outcome is consistent with the higher
320 heterogeneity displayed by the former sample, where the spatial distribution of Y_{r_i} is affected by an
321 increased level of uncertainty as compared to its Berea-based counterpart.

322 Otherwise, two distinct behaviors emerge with regard to the location of the peak(s) of the
323 distributions: (i) the location of the peak of the distributions is virtually insensitive to r_i for the Berea;
324 while (ii) the two peaks of the bimodal distributions of the Topopah sample display a clear tendency
325 to migrate towards higher permeability values as r_i increases. These observations are consistent with
326 the homogeneous nature of the Berea and the two-material (pumice and matrix being high and low
327 permeable, respectively) type of heterogeneity displayed by the Topopah sample. It is also in line
328 with the previously noted weak sensitivity of the MSP measurements to region of low permeability.
329 With reference to the Berea sample, if a measurement taken at a given location with a small r_i is close

330 to the average value (i.e., Y_{r_i} is close to zero in our setting), it is likely that the same behavior is
 331 observed also for larger r_i due to the homogeneity of the sample. Otherwise, in the case of the
 332 Topopah sample there are more chances that increasing r_i (hence involving larger volumes of the
 333 rock) yields a shift of the ensuing measurements toward higher values.

334 Inspection of Figure 3d reveals that, given a reference support scale r_i , the mutual information
 335 shared with measurements taken at larger support scales r_j decreases with increasing r_j for both
 336 rock samples. In other words, the representativeness for system characterization of the sets of data
 337 associated with increasingly coarse support scale diminishes, as compared to the data collected at the
 338 given reference scale. At the same time, we note that the way in which $I^*(Y_{r_i}; Y_{r_j})$ decreases with r_j
 339 is very similar for (i) the two analyzed reference support scales, i.e., r_1 and r_2 , and (ii) for the two
 340 considered rock types. We interpret this result as a sign of (at least qualitative) consistency in the way
 341 information is shared between datasets of measurements associated with increasing size of r_i , despite
 342 the different geological nature of the two types of samples analyzed. Otherwise, Figure 3d indicates
 343 that the (normalized) mutual information $I^*(Y_{r_i}; Y_{r_j})$ is always lower in the Topopah than in the Berea
 344 system. This result provides a quantification of the qualitative observation that there is an overall
 345 decrease of the representativeness of the datasets associated with increasing data support (with respect
 346 to data collected with smaller r_i) as the system heterogeneity becomes stronger.

347 Figure 4 depicts the results of the information partitioning procedure detailed in Section 2.3
 348 considering the Berea sample and two triplets of datasets $(Y_{r_{i+1}}, Y_{r_{i+2}}; Y_{r_i})$, with $r_i =$ (a) r_1 and (b) r_2 .
 349 Corresponding results for the Topopah sample are depicted in (c) for $r_i = r_1$ and (d) for $r_i = r_2$. For
 350 ease of comparison between the results, we normalize the unique, synergetic and redundant
 351 contributions in (4) by the multivariate mutual information of the corresponding triplet, e.g.,
 352 $U^*(Y_{r_{i+1}}; Y_{r_i}) = U(Y_{r_{i+1}}; Y_{r_i}) / I(Y_{r_{i+1}}, Y_{r_{i+2}}; Y_{r_i})$, $U^*(Y_{r_{i+2}}; Y_{r_i}) = U(Y_{r_{i+2}}; Y_{r_i}) / I(Y_{r_{i+1}}, Y_{r_{i+2}}; Y_{r_i})$;
 353 $R^*(Y_{r_{i+1}}, Y_{r_{i+2}}; Y_{r_i}) = R(Y_{r_{i+1}}, Y_{r_{i+2}}; Y_{r_i}) / I(Y_{r_{i+1}}, Y_{r_{i+2}}; Y_{r_i})$, $S^*(Y_{r_{i+1}}, Y_{r_{i+2}}; Y_{r_i}) = S(Y_{r_{i+1}}, Y_{r_{i+2}}; Y_{r_i}) / I(Y_{r_{i+1}}, Y_{r_{i+2}}; Y_{r_i})$.
 354 Results in Figure 4a-b suggest that for the Berea sample: (i) most of the multivariate information is
 355 redundant, a finding that can be linked to the dependence detected between the sets of data associated
 356 with the two coarser support scales (see, e.g., Figure 3d); (ii) the synergetic information is practically
 357 zero for both triplets considered, i.e., the simultaneous knowledge of the system at two coarser scales
 358 does not provide any additional information; (iii) data associated with the middle (in the triplets)
 359 support scale provides a non-negligible unique information content, the latter being less pronounced
 360 for the data referring to the most coarse support (in the triples). These results (i.e., high redundancy
 361 and high/low uniqueness for the middle/largest support scale) suggest that, considering the depiction
 362 of the system rendered at the finest support scale, the information provided by the investigations at
 363 the coarsest support scale is mostly contained by the information provided by the data collected at the
 364 intermediate scale. This element suggests a nested nature of the information linked to data collected
 365 at progressively increasing scales with respect to the information contained in the data associated
 366 with the smallest support scale. This finding can be linked to the homogeneous nature of the Berea
 367 sample, whereas the characterization at diverse scales does not change dramatically (e.g., note the
 368 similarities in the spatial patterns of Y_{r_i} in Figure 1 for the Berea sample as a function of r_i), thus

369 promoting (a) the redundancy of information associated with measurements at the intermediate and
370 larger scales and (b) the uniqueness of information revealed for the intermediate scale.

371 Otherwise, inspection of Figure 4c-d reveals that for the Topopah rock sample: (i) most of the
372 multivariate information coincides with the unique information associated with the intermediate
373 scale; (ii) the redundant and unique contribution associated with the largest scale are still non-
374 negligible, yet being substantially smaller than the uniqueness contribution provided by the
375 intermediate scale; (iii) there is practically no synergetic information. This set of results descends
376 from the moderate or marked discrepancies displayed by Y_{r_i} data as r_i increases by one or two sizes,
377 respectively (e.g., see the faces depicted in Figure 1 for the Topopah sample). In other words, relying
378 on a device such as the MSP to obtain permeability data enables sampling a volume of the rock
379 according to which the majority of the multivariate information in a triplet is associated with a
380 significant unique contribution of the intermediate scale, the information related to the largest scale
381 still being weakly unique and weakly redundant.

382 5. Discussion

383 We recall that the focus of the present study is the quantification of the information content and
384 information shared between pairs and triplets of datasets of air permeability observations associated
385 with diverse sizes of the measurement/support scale. We exemplify our analysis upon relying on data
386 collected across two different types of rocks, i.e., a Berea and a Topopah sample, that are
387 characterized by different degrees of heterogeneity.

388 These datasets (or part of these) have been considered in some prior studies. Tidwell and Wilson
389 (1999a, b) and Lowry and Tidwell (2005) assess the impact of the size of the support/measurement
390 scale on key summary one-point (i.e., mean and variance) and two-points (i.e., variogram) statistics
391 within the context of classical geostatistical methods and evaluate kriging-based estimates of the
392 underlying random fields. Siena et al. (2012) and Riva et al. (2013) analyze the scaling behavior of
393 the main statistics of the log permeability data and of their increments (i.e., sample structure functions
394 of various orders), with emphasis on the assessment of power-law scaling behavior. On these bases,
395 Riva et al. (2013) conclude that the data related to the Berea sample can be interpreted as observations
396 from a sub-Gaussian random field subordinated to truncated fractional Brownian motion or Gaussian
397 noise. All of these studies focus on (a) the geostatistical interpretation of the behavior displayed by
398 the probability density function (and key moments) of the data and their spatial increments and (b)
399 the analysis of the skill of selected models to interpret the observed behavior of the main statistical
400 descriptors evaluated upon considering separately data associated with diverse measurement/support
401 scale. Furthermore, Tidwell and Wilson (2002) analyzed the Berea and Topopah datasets (considering
402 separately data characterized by diverse support scales) to assess possible correspondences between
403 the permeability field and some attributes of the rock samples determined visually through digital
404 imaging and conclude that image analysis can assist delineation of spatial patterns of permeability.

405 We remark that in all of the studies mentioned above the datasets associated with a given
406 support (or measurement) scale are analyzed separately. Otherwise, we leverage on elements of IT,
407 which allow a unique opportunity to circumvent limitations of linear metrics (e.g., Pearson
408 correlation) and analyze the relationships (in terms of shared amount of information) between pairs
409 (i.e., bivariate mutual information) or triplets (i.e., multivariate mutual information) of variables. We
410 also note that, even as visual inspection of $p(Y_{r_i})$ associated with diverse sizes of the support scale r_i
411 (see Figure 3a and Figure 3b for the Berea and Topopah, respectively) can show that these probability
412 densities can be intuitively linked to the documented decrease of the corresponding Shannon entropies

413 with increasing r_i (see Figure 3c and Section 4), it would be hard to readily infer from such a visual
414 comparative inspection the behavior of the bivariate (see Figure 3d) and multivariate (see Figure 4)
415 mutual information because these require (see Eq.s (2)-(8)) the evaluation of the joint probability
416 mass functions.

417 Considering an operational context, including, e.g., groundwater resource management or
418 (conventional/unconventional) oil recovery, we observe that it is common to have at our disposal
419 permeability data associated with diverse support scales. These can be inferred from, e.g., large scale
420 pumping tests, downhole impeller flowmeter measurements, core flood experiments at the laboratory
421 scale, geophysical investigations, or particle-size curves (see e.g., Paillet, 1989; Oliver, 1990; Dykaar
422 and Kitanidis, 1992; Harvey, 1992; Deutsch and Journel, 1994; Day-Lewis et al., 2000; Zhang and
423 Winter, 2000; Attinger, 2003; Pavelic et al., 2006; Neuman et al., 2008; Riva et al., 2009; Barahona-
424 Palomo et al., 2011; Quinn et al., 2012; Shapiro et al., 2015; Galvão et al., 2016; Menafoglio et al.,
425 2016; Medici et al., 2017; Dausse et al., 2019, and reference therein). Assessing (i) the information
426 content and (ii) the amount of information shared between permeability data associated with differing
427 support scales (and/or diverse measuring devices/techniques) along the lines illustrated in the present
428 study can be beneficial to obtain a quantitative appraisal of possible feedbacks among diverse
429 approaches employed for aquifer/reservoir characterization. Results of such an analysis can
430 potentially serve as a guidance for the screening of datasets which are most informative to provide a
431 comprehensive description of the spatially heterogeneous distribution of permeability. While the
432 methodology detailed in Section 3 is readily transferable to scenarios where multi-scale permeability
433 are available, the appraisal of the general nature of some specific findings of the present study (e.g.,
434 decrease of the Shannon entropy as the support scale increases, regularity in the trends displayed by
435 the normalized bivariate mutual information) still remains an open issue which will be the subject of
436 future works.

437

6. Conclusions

438 We rely on elements of Information Theory to interpret multi-scale permeability data collected
439 over blocks of Berea Sandstone and a Topopah Spring Tuff, representing a nearly homogeneous and
440 a heterogeneous porous medium composed of a two-material mixture, respectively. The unique multi-
441 scale nature of the data enables us to quantify the way information is shared across measurement
442 scales, clearly identifying information losses and/or redundancies that can be associated with the joint
443 use of permeability data collected at differing scales. Our study leads to the following major
444 conclusions:

- 445 1. An increase in the characteristic length associated with the scale at which the laboratory scale
446 (normalized) gas permeability data are collected corresponds to a quantifiable decrease in the
447 Shannon entropy of the associated probability mass function. This result is consistent with
448 the qualitative observation that the ability of capturing the degree of spatial heterogeneity of
449 the system decreases as the data support scale increases.
- 450 2. The (normalized) bivariate mutual information shared between pairs of permeability datasets
451 collected at (i) a fixed fine scale (taken as reference) and (ii) larger scales decreases in a
452 mostly regular fashion independent from the size of the reference scale, once the bivariate
453 mutual information is normalized by the Shannon entropy of the data taken at the reference
454 scale. This result highlights a consistency in the way information associated with data at
455 diverse scales is shared for the instrument and the porous systems here analyzed.
- 456 3. As the degree of heterogeneity of the system increases, we document a corresponding
457 increase in the Shannon entropy (given a support scale) and a decrease in the values of the

- 458 normalized bivariate mutual information (given two support scales) between permeability
459 data collected at the differing measurement scales.
- 460 4. Results of the information partitioning of the multivariate mutual information shared by
461 permeability data collected at three increasing support scales for the Berea sandstone sample
462 exhibit a marked level of redundancy and high/low uniqueness for the data collected at the
463 intermediate/coarser scale in the triplets with respect to the data associated with the finest
464 scale. This result can be linked to the fairly homogeneous nature of the sample, that is also
465 reflected in the moderate variation of the observed (normalized) gas permeability values with
466 increasing size of the support scale.
 - 467 5. Information partitioning for the Topopah tuff sample indicates the occurrence of a still
468 significant amount of unique information associated with the data collected at the
469 intermediate scale, while the redundant portion and the unique contribution linked to the
470 largest scale in a triplet are clearly diminished. This result descends from the heterogeneous
471 structure of the Topopah porous system, where the recorded (normalized) gas permeabilities
472 display moderate or marked discrepancies as r_i increases by one or two sizes, respectively.
 - 473 6. For both rock samples considered, the simultaneous knowledge of permeability data taken at
474 the intermediate and coarser support scales in a triplet does not provide significant additional
475 information with respect to that already contained in the data taken at the fine scale, i.e., the
476 synergic contribution in the resulting datasets is virtually zero.

477 Given the nature of the approach we employ, the latter is potentially amenable to be transferred to
478 analyze settings involving other kinds of datasets associated with diverse hydrogeological quantities
479 (including, e.g., porosity or sorption/desorption parameters) or considering measurement/sampling
480 devices of a diverse design. Future developments could also include exploring the possibility of
481 embedding the approach within the workflow of optimal experimental design and/or data-worth
482 analysis strategies.

483 **Data Availability**

484 Data employed were graciously provided by Tidwell, V.C., and are available online
485 (<https://data.mendeley.com/datasets/ygcv32nw5/1>).

486 **Author contributions**

487 The methodology was developed by AD, supervised by and discussed with AG and MR. All codes
488 were developed by AD. The manuscript was drafted by AD. Structure, narrative and language of the
489 manuscript were revised and significantly improved by AG and MR.

490 **Competing interests**

491 The authors declare to have no competing interests.

492

493 **Acknowledgements**

494 The authors would like to thank the EU and MIUR for funding, in the frame of the collaborative
495 international Consortium (WE-NEED) financed under the ERA-NET WaterWorks2014 Cofunded
496 Call. This ERA-NET is an integral part of the 2015 Joint Activities developed by the Water
497 Challenges for a Changing World Joint Programme Initiative (Water JPI). Prof. A. Guadagnini
498 acknowledges funding from Région Grand-Est and Strasbourg-Eurométropole through the ‘Chair
499 Gutenberg’.

500

501 **References**

- 502 Andersson, J. E., Ekman, L., Gustafsson, E., Nordqvist, R., and Tiren, S.: Hydraulic interference tests
503 and tracer tests within the Brändöan area, Finnsjon study site, the fracture zone project-Phase 3,
504 Technical Report 89-12, Sweden Nuclear Fuel and Waste Management Company, Stockholm, 1988.
- 505 Attinger, S.: Generalized coarse graining procedures for flow in porous media, *Computational Geosc.*,
506 7, 253-273. doi:10.1023/B:COMG.0000005243.73381.e3, 2003.
- 507 Barahona-Palomo, M., Riva, M., Sanchez-Vila, X., Vazquez-Sune, E., and Guadagnini, A.:
508 Quantitative comparison of impeller flowmeter and particle-size distribution techniques for the
509 characterization of hydraulic conductivity variability, *Hydrogeol. J.*, 19(3), 603-612.
510 doi:10.1007/s10040-011-0706-5, 2011.
- 511 Beckie, R.: A comparison of methods to determine measurement support volumes, *Water Resour.*
512 *Res.*, 37(4), 925-936. <https://doi.org/10.1029/2000WR900366>, 925-936.
- 513 Bertschinger, N., Rauh, J., Olbrich, E., Jost, J., and Ay, N.: Quantifying unique information, *Entropy*,
514 16(4), 2161-2183, doi:10.3390/e16042161, 2014.
- 515 Bianchi, M., and Pedretti, D.: Geological entropy and solute transport in heterogeneous porous media,
516 *Water Resour. Res.*, 53, 4691-4708, doi:10.1002/2016WR020195, 2017.
- 517 Bianchi, M., and Pedretti, D.: An entrogram-based approach to describe spatial heterogeneity with
518 applications to solute transport in porous media, *Water Resour. Res.*, 54, 4432-4448.
519 <https://doi.org/10.1029/2018WR022827>, 2018
- 520 Boso, F., and Tartakovsky, D. M.: Information-theoretic approach to bidirectional scaling, *Water*
521 *Resour. Res.*, 54, 4916–4928. <https://doi.org/10.1029/2017WR021993>, 2018.
- 522 Brace, W. F.: Permeability of crystalline rocks: New in situ measurements, *J. Geophys. Res.*, 89 (B6),
523 4327-4330, <https://doi.org/10.1029/JB089iB06p04327>, 1984.
- 524 Butera, I., Vallivero, L., and Rodolfi, L.: Mutual information analysis to approach nonlinearity in
525 groundwater stochastic fields, *Stoch. Environ. Res. Risk Assess.*, 32 (10), 2933-2942,
526 <https://doi.org/10.1007/s00477-018-1591-4>, 2018.
- 527 Cintoli, S., Neuman, S. P., and Di Federico, V.: Generating and scaling fractional Brownian motion
528 on finite domains, *Geophys. Res. Lett.*, 32, 8, <https://doi.org/10.1029/2005GL022608>, 2005
529
- 530 Clauser, C.: Permeability of crystalline rocks, *Eos Transport*, AGU 73(21), 233, 1992.
- 531 Cover, T. M., and Thomas, J. A.: *Elements of Information Theory*, John Wiley, Hoboken, N. J., 2006.
- 532 Dausse, A., Leonardi, V., and Jourde, H.: Hydraulic characterization and identification of flow-
533 bearing structures based on multiscale investigations applied to the Lez karst aquifer, *J. Hydrol.:*
534 *Regional Studies*, 26, 100627. <https://doi.org/10.1016/j.ejrh.2019.100627>, 2019.
- 535 Deutsch, C. V., and Journel, A. G.: Integrating well test derived effective absolute conductivities in
536 geostatistical reservoir modeling, in: *Stochastic Modeling and Geostatistics: Principles, Methods and*
537 *Case Studies*, eds. J. Yarus and R. Chambers, AAPG Computer Applications in Geology, No. 3, pp.
538 131–142. Amer. Assoc. of Petrol. Geol., Tulsa, 1994.

539 Dykaar, B. B., and Kitanidis, P. K.: Determination of the effective hydraulic conductivity for
540 heterogeneous porous media using a numerical spectral approach, 1. Methods, *Water Resour. Res.*,
541 28(4), 1155-1166. <https://doi.org/10.1029/91WR03084>, 1992.

542 Dykaar, B. B., and Kitanidis, P. K.: Determination of the effective hydraulic conductivity for
543 heterogeneous porous media using a numerical spectral approach, 2. Results, *Water Resour. Res.*,
544 28(4), 1167-1178. <https://doi.org/10.1029/91WR03083>, 1992.

545 Galvão, P., Halihan, T., and Hirata, R.: The karst permeability scale effect of Sete Lagos, MG, Brazil,
546 *J. Hydrol.*, 532, 149-162. <https://doi.org/10.1016/j.jhydrol.2015.11.026>, 2016.
547

548 Goggin, D. J., Thrasher, R. L., and Lake, L. W.: A theoretical and experimental analysis of
549 minipermeameter response including gas slippage and high velocity flow effects, *In Situ*, 12, 79-116,
550 1988.
551

552 Gong, W., Gupta, H. V., Yang, D., Sricharan, K., and Hero III, A. O.: Estimating epistemic and
553 aleatory uncertainties during hydrologic modeling: An information theoretic approach, *Water Resour.*
554 *Res.*, 49, 2253-2273. doi:10.1002/wrcr.20161, 2013.
555

556 Gong, W., Yang, D., Gupta, H. V. and Nearing, G.: Estimating information entropy for hydrological
557 data: One-dimensional case, *Water Resour. Res.*, 50(6), 5003–5018, doi:10.1002/2014WR015874,
558 2014.
559

560 Goodwell, A. E., and Kumar, P.: Temporal information partitioning: Characterizing synergy,
561 uniqueness, and redundancy in interacting environmental variables, *Water Resour. Res.*, 53,
562 doi:10.1002/2016WR020216, 2017.
563

564 Gotovac, H., Cvetkovic, V., and Andrievic, R.: Significance of higher moments for complete
565 characterization of the travel time probability density function in heterogeneous porous media using
566 the maximum entropy principle, *Water Resour. Res.* 46, W05502.
567 <https://doi.org/10.1029/2009WR008220>, 2010.
568

569 Griffith, V., and Ho, T.: Quantifying redundant information in predicting a target random variable,
570 *Entropy*, 17(7), 4644-4653, doi:10.3390/e17074644, 2015.
571

572 Griffith, V., and Koch, C.: Quantifying synergistic mutual information, *Guided Self-Organization:*
573 *Inception*, edited by M. Prokopenko, 159–190, Springer-Verlag Berlin Heidelberg, Berlin,
574 Germany, 2014.
575

576 Guadagnini, A., Neuman, S. P., Schaap, M. G., and Riva, M.: Anisotropic statistical scaling of vadose
577 zone hydraulic property estimates near Maricopa, Arizona, *Water Resour. Res.*, 49, 1-17.
578 doi:10.1002/2013WR014286, 2013
579

580 Guadagnini, A., Riva, M., and Neuman, S. P.: Recent advances in scalable non-Gaussian
581 geostatistics: the generalized sub-Gaussian model, *J. Hydrol.*, 562, 685-691.
582 doi:10.1016/j.jhydrol.2018.05.001, 2018.
583

584 Guzman, A., Neuman, S. P., Lohrstorfer, C., and Bassett, R. L.: Validation studies for assessing flow
585 and transport through unsaturated fractured rocks, edited by R. L. Bassett et al. Rep. NUREG/CR-
586 6203, chapter 4, U.S. Nuclear Regulatory Commission, Washington, D. C, 1994.

587 Guzman, A. G., Geddis, A. M., Henrich, M. J., Lohrstorfer, C. F., and Neuman, S. P.: Summary of
588 air permeability data from single-hole injection tests in unsaturated fractured tuffs at the Apache Leap
589 research site: Results of steady state test interpretation. Rep. NUREG/CR-6360, U.S. Nuclear
590 Regulatory Commission, Washington, D. C, 1996.

591 Harder, M., Salge, C., and Polani, D.: Bivariate measure of redundant information. *Phys. Rev. E*,
592 87(1), 012130. doi:10.1103/PhysRevE.87.012130, 2013.

593
594 Harvey, C. F.: Interpreting parameter estimates obtained from slug tests in heterogeneous aquifers,
595 M. S. thesis, Appl. Earth Science Department, Stanford University, Stanford. 1992

596
597 Hyun, Y., Neuman, S.P., Vesselinov, V. V., Illman, W. A., Tartakovsky, D. M., and Di Federico, V.:
598 Theoretical interpretation of a pronounced permeability scale effect in unsaturated fractured tuff,
599 *Water Resour. Res.*, 38(6), 1092. doi:10.1029/2002WR000658, 2002.

600
601 Illman, W. A.: Analysis of permeability scaling within single boreholes, *Geophys. Res. Lett.*, 31,
602 L06503. doi:10.1029/2003GL019303, 2004.

603 Kitanidis, P. K.: The concept of the dilution index, *Water Resour. Res.* 30(7), 2011-2016.
604 <https://doi.org/10.1029/94WR00762>, 1994.

605 Loritz, R., Gupta, H., Jackisch, C., Westhoff, M., Kleidon, A., Ehret, U. and Zehe, E.: On the dynamic
606 nature of hydrological similarity, *Hydrol. Earth Syst. Sci.*, 22(7), 3663–3684, doi:10.5194/hess-22-
607 3663-2018, 2018.

608 Lowry, T. S., and Tidwell, V. C.: Investigation of permeability upscaling experiments using
609 deterministic modeling and monte carlo analysis, World Water and Environmental Resources
610 Congress 2005, May 15-19, Anchorage, Alaska, United States.
611 [https://doi.org/10.1061/40792\(173\)372](https://doi.org/10.1061/40792(173)372), 2005.

612 Mälicke, M., Hassler, S. K., Blume, T., Weiler, M., and Zehe, E.: Soil moisture: variable in space but
613 redundant in time, *Hydrology and Earth System Sciences*, under discussion,
614 <https://doi.org/10.5194/hess-2019-574>, 2019.

615 Maréchal, J. C., Dewandel, B., and Subrahmanyam, K.: Use of hydraulic tests at different scales to
616 characterize fracture network properties in the weathered-fractured layer of a hard rock aquifer, *Water*
617 *Resour. Res.*, 40, W11508. doi:10.1029/ 2004WR003137, 2004.

618
619 Medici, G., West, L. J., Mountney, N. P.: Characterization of a fluvial aquifer at a range of depths
620 and scales: the Triassic St. Bees sandstone formation, Cumbria, UK, *Hydrogeol. J.*, 26, 565-591.
621 <https://doi.org/10.1007/s10040-017-1676-z>, 2018.

622 Menafoglio, A., Guadagnini, A., and Secchi, P.: A Class-Kriging predictor for functional
623 compositions with application to particle-size curves in heterogeneous aquifers, *Math. Geosci.*, 48,
624 463-485. doi:10.1007/s11004-015-9625-7, 2016.

625 Mishra, S., Deeds, N., and Ruskauff, G.: Global sensitivity analysis techniques for probabilistic
626 ground water modeling. *Ground Water* 47(5), 730-747. doi:10.1111/j.1745-6584.2009.00604.x,
627 2009.

628 Molz, F., Dinwiddie, C. L., and Wilson, J. L.: A physical basis for calculating instrument spatial
629 weighting functions in homogeneous systems, *Water Resour. Res.*, 39(4), 1096.
630 doi:10.1029/2001WR001220, 2003.

631 Nearing, G. S., Ruddell, B. J., Clark, P. M., Nijssen, B., and Peters-Lidard, C. D.: Benchmarking and
632 process diagnostic of land models, *J. Hydrometeor.*, 19, 1835-1852, <https://doi.org/10.1175/JHM-D-17-0209.1>, 2018.

633
634

635 Neuman, S. P.: Generalized scaling of permeabilities: Validation and effect of support scale,
636 *Geophys. Res. Lett.*, 21(5), 349-352, <https://doi.org/10.1029/94GL00308>, 1994.

637

638 Neuman, S. P., and Di Federico, V.: Multifaceted nature of hydrogeologic scaling and its
639 interpretation, *Rev. Geophys.*, 41, 1014. doi:10.1029/2003RG000130, 2003.

640 Neuman, S. P., Riva, M., and Guadagnini, A.: On the geostatistical characterization of hierarchical
641 media, *Water Resour. Res.*, 44, W02403. doi:10.1029/2007WR006228, 2008.

642 Nowak, W., and Guthke, A.: Entropy-based experimental design for optimal model discrimination in
643 the geosciences, *Entropy*, 18, 409. doi:10.3390/e18110409, 2016.

644 Olbrich, E., Bertschinger, N., and Rauh, J.: Information decomposition and synergy, *Entropy*, 11,
645 3501-3517. doi:10.3390/e17053501, 2015.

646 Oliver, D. S.: The averaging process in permeability estimation from well-test data, *SPE Form Eval.*,
647 5, 319-324. <https://doi.org/10.2118/19845-PA>, 1990.

648 Paillet, P. L.: Analysis of geophysical well logs and flowmeter measurements in borehole penetrating
649 subhorizontal fracture zones, Lac du Bonnet Batholith, Manitoba, Canada, U.S. Geological Survey,
650 Water-Resources investigation report 89, 4211. 1989.

651 Pavelic, P., Dillon, P., and Simmons, C. T.: Multiscale characterization of a heterogeneous aquifer
652 using an ASR operation, *Ground Water*, 44(2), 155-164. doi:10.1111/j.1745-6584.2005.00135.x,
653 2006.

654 Quinn, P., Cherry, J. A., and Parker, B. L.: Hydraulic testing using a versatile straddle packer system
655 for improved transmissivity estimation in fractured-rock boreholes, *Hydrogeol. J.*, 20, 1529-1547.

656 Riva, M., Neuman, S. P., Guadagnini, A., and Siena, S.: Anisotropic scaling of Berea sandstone log
657 air permeability statistics, *Vadose Zone J.*, 12, 1-15. doi:10.2136/vzj2012.0153, 2013.

658

659 Rovey, C. W., and Cherkauer, D. S.: Scale dependency of hydraulic conductivity measurements,
660 *Ground Water*, 33 (5), 769-780, <https://doi.org/10.1111/j.1745-6584.1995.tb00023.x>, 1995.

661

662 Ruddell, B. L., and Kumar, P.: Ecohydrologic process networks: 1. Identification, *Water Resour.*
663 *Res.*, 45, W03419. doi:10.1029/2008WR007279, 2009.

664

665 Sanchez-Vila, X., Carrera, J., and Girardi, J. P.: Scale effects in transmissivity, *J. Hydrol.*, 183, 1-22,
666 [https://doi.org/10.1016/S0022-1694\(96\)80031-X](https://doi.org/10.1016/S0022-1694(96)80031-X), 1996.

667 Schulze-Makuch, D., and Cherkauer, D. S.: Variations in hydraulic conductivity with scale of
668 measurements during aquifer tests in heterogenous, porous carbonate rock, *Hydrogeol. J.*, 6, 204-215,
669 <https://doi.org/10.1007/s100400050145>, 1998.

670

671 Schad, H., and Teutsch, G.: Effects of the investigation scale on pumping test results in heterogeneous
672 porous aquifers, *J. Hydrol.*, 159 (1-4), 61-77, [https://doi.org/10.1016/0022-1694\(94\)90249-6](https://doi.org/10.1016/0022-1694(94)90249-6), 1994.

673 Schulze-Makuch, D., Carlson, D. A., Cherkauer, D. S., and Malik, P.: Scale dependency of hydraulic
674 conductivity in heterogeneous media, *Ground Water*, 37, 904-919, <https://doi.org/10.1111/j.1745-6584.1999.tb01190.x>, 1999.

675
676

677 Shannon, C.: A mathematical theory of communication, *Bell Syst. Tech. J.*, 27(3).
678 doi:10.1002/j.1538-7305.1948.tb01338.x, 1948.

679

680 Shapiro, A. M., Ladderud, J. A., and Yager, R. M.: Interpretation of hydraulic conductivity in a
681 fractured-rock aquifer over increasingly larger length dimensions, *Hydrogel. J.*, 23, 1319-1339. doi:
682 10.1007/s10040-015-1285-7, 2015.

683

684 Siena, M., Guadagnini, A., Riva, M., and Neuman, S. P.: extended power-law scaling of air
685 permeabilities measured on a block of tuff, *Hydrol. Earth Syst. Sci.*, 16, 29-42, doi:10.5194/hess-16-
686 29-2012, 2012.

687

688 Stone, J. V.: *Information Theory: A Tutorial Introduction*. Sebtel Press, 2015.

689

690 Tartakovsky, D. M., Moulton, J. D., and Zlotnik, V. A.: Kinematic structure of minipermeameter
691 flow, *Water Resour. Res.*, 36(9), 2433-2442, <https://doi.org/10.1029/2000WR900178>, 2000.

692

693 Tidwell, V. C., and Wilson, J. L.: Laboratory method for investigating permeability upscaling, *Water
Resour. Res.*, 33(7), 1607-1616, <https://doi.org/10.1029/97WR00804>, 1997.

694

695 Tidwell, V. C., and Wilson, J. L.: Permeability upscaling measured on a block of Berea Sandstone:
696 Results and interpretation, *Math. Geol.*, 31(7), 749-769, <https://doi.org/10.1023/A:1007568632217>,
1999a.

697

698 Tidwell, V. C., and Wilson, J. L.: Upscaling experiments conducted on a block of volcanic tuff:
699 Results for a bimodal permeability distribution, *Water Resour. Res.*, 35(11), 3375-3387,
700 <https://doi.org/10.1029/1999WR900161>, 1999b.

701

702 Tidwell, V. C., and Wilson, J. L.: Heterogeneity, permeability patterns, and permeability upscaling:
703 Physical characterization of a block of Massillon Sandstone exhibiting nested scales of heterogeneity,
704 *SPE Reser. Eval. Eng.*, 3(4), 283-291, <https://doi.org/10.2118/65282-PA>, 2000.

705

706 Tidwell, V. C., and Wilson, J. L.: Visual attributes of a rock and their relationship to permeability: A
707 comparison of digital image and minipermeameter data, *Water Resour. Res.*, 38(11), 1261.
708 doi:10.1029/2001WR000932, 2002.

709

710 Vesselinov, V. V., Neuman, S. P., and Illman, W. A.: Three-dimensional numerical inversion of
711 pneumatic cross-hole tests in unsaturated fractured tuff: 1. Methodology and borehole effects, *Water
Resour. Res.*, 37(12), 3001-3018, <https://doi.org/10.1029/2000WR000133>, 2001a.

712

713 Vesselinov, V. V., Neuman, S. P., and Illman, W. A.: Three-dimensional numerical inversion of
714 pneumatic cross-hole tests in unsaturated fractured tuff: 2. Equivalent parameters, high-resolution
715 stochastic imaging and scale effects, *Water Resour. Res.*, 37(12), 3019-3042,
716 <https://doi.org/10.1029/2000WR000135>, 2001b.

717

718 Wellman, F. J., and Regenaur-Lieb, K.: Uncertainties have a meaning: Information entropy as a
719 quality measure for 3-D geological models, *Tectonophys.*, 526-529, 207-216.
720 doi:10.1016/j.tecto.2011.05.001, 2012.
721

722 Wellman, F. J.: Information theory for correlation analysis and estimation of uncertainty reduction in
723 maps and models, *Entropy*, 15, 1464-1485. doi:10.3390/e15041464, 2013.
724

725 Winter, C. L., and Tartakovsky, D. M.: Theoretical foundation for conductivity scaling, *Geophys.*
726 *Res. Lett.*, 28(23), 4367-4369, doi:10.1029/2001GL013680, 2001.

727 Williams, P. L., and Beer, R. D.: Nonnegative decomposition of multivariate information, *CoRR.*,
728 <http://arxiv.org/abs/1004.2515>, 2010.
729

730 Woodbury, A. D., and Ulrych, T. J.: Minimum relative entropy: forward probabilistic modeling,
731 *Water Resour. Res.* 29(8), 2847-2860. <https://doi.org/10.1029/93WR00923>, 1993.
732

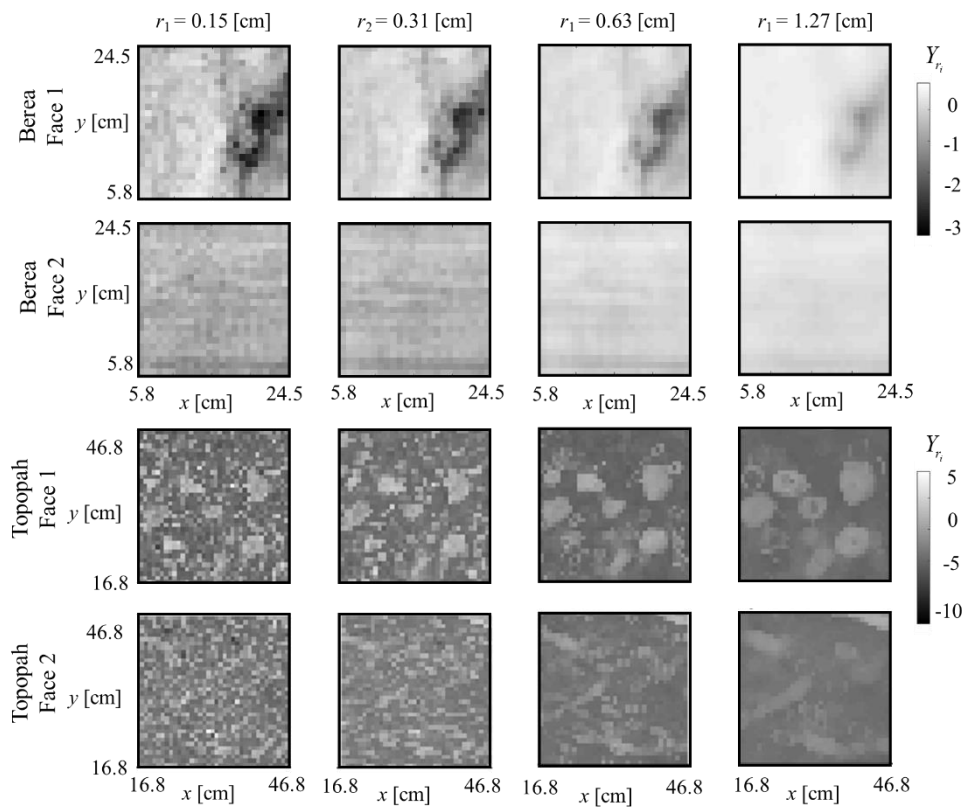
733 Woodbury, A. D., and Ulrych, T. J.: Minimum relative entropy inversion: theory and application to
734 recovering the release history of a groundwater contaminant, *Water Resour. Res.* 32(9), 2671-2681.
735 <https://doi.org/10.1029/95WR03818>, 1996.
736

737 Woodbury, A. D., and Ulrych, T. J.: A full-Bayesian approach to the groundwater inverse problem
738 for steady state flow, *Water Resour. Res.* 36(8), 2081-2093. <https://doi.org/10.1029/2000WR900086>,
739 2000.
740

741 Zeng, X. K., Wan, D., and Wu, J. C.: Sensitivity analysis of the probability distribution of
742 groundwater level series based on information entropy, *Stoch. Environ. Res. Risk. Assess* 26, 345-
743 356. <https://doi.org/10.1007/s00477-012-0556-2>, 2012.
744

745 Zhang, D., and Winter, C. L.: Theory, modeling and field investigation in Hydrogeology: A special
746 volume in honor of Shlomo P. Neuman's 60th birthday, Special paper, Geological Society of America,
747 Boulder, Colorado, 2000.
748

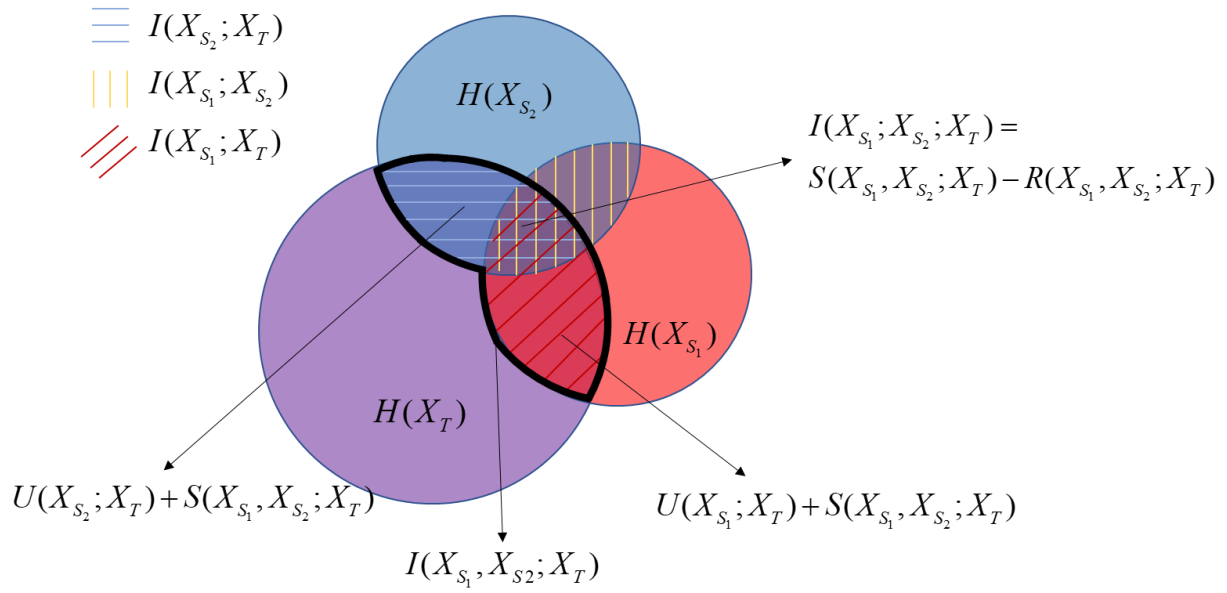
749 Zlotnik, V. A., Zurbuchen, B. R., Ptak, T., and Teutsch, G.: Support volume and scale effect in
750 hydraulic conductivity: experimental aspects. In: Zhang, D., Winter, C.L. (Eds.), *Theory, Modeling,*
751 *and Field Investigation in Hydrogeology: A Special Volume in Honor of Shlomo P. Neuman's 60th*
752 *Birthday*, Boulder, CO, Geological Society of America Special Paper 348, pp. 191-213, 2000.
753



755

756 Figure 1. Examples of spatial distributions of the natural logarithm of normalized gas permeability,
 757 Y_r , for two faces of a cubic block of Berea Sandstone (first and second rows) and Topopah Spring
 758 Tuff (third and fourth rows) taken with four increasing support scales (columns, left to right).

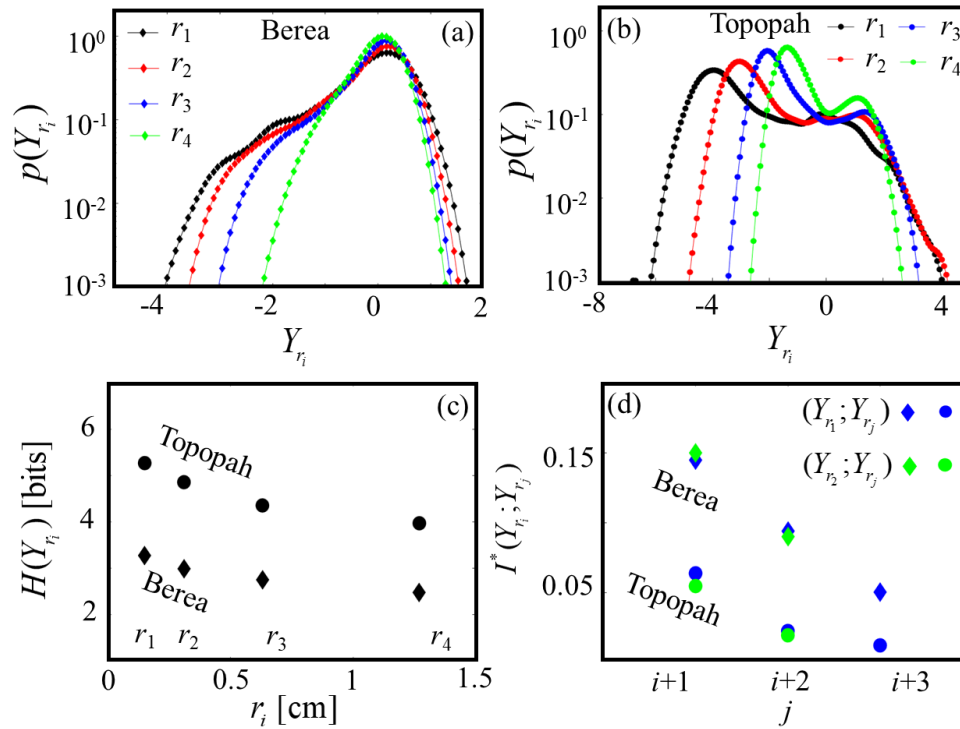
759



760

761 Figure 2. Venn diagram representation of the Information Theory concepts considering two sources,
 762 i.e., X_{S_1} and X_{S_2} , and a target variable, X_T . Areas of the circles are proportional to Shannon entropy
 763 (i.e., $H(X_{S_1})$, $H(X_{S_2})$ and $H(X_T)$); overlaps of pairs of circles reflect bivariate mutual information
 764 (i.e., $I(X_{S_1}; X_T)$, $I(X_{S_2}; X_T)$, and $I(X_{S_1}; X_{S_2})$); and the strength of the multivariate mutual
 765 information (i.e., $I(X_{S_1}, X_{S_2}; X_T)$) corresponds to the region delimited by the thick black curve.
 766 Unique (i.e., $U(X_{S_1}; X_T)$ and $U(X_{S_2}; X_T)$), synergetic (i.e., $S(X_{S_1}, X_{S_2}; X_T)$), and redundant (i.e.,
 767 $R(X_{S_1}, X_{S_2}; X_T)$) components are also highlighted, as well as the interaction information (i.e.,
 768 $I(X_{S_1}; X_{S_2}; X_T)$).

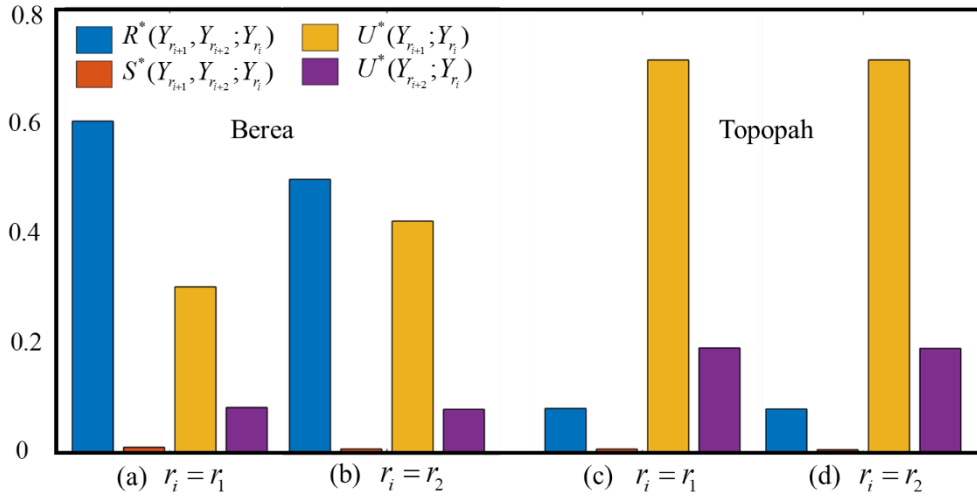
769



771

772 Figure 3. Probability mass function of the logarithm of normalized gas permeability, $p(Y_{r_i})$, for
 773 various support scale, r_i ($i = 1$ (black), 2 (red), 3 (blue), 4 (green)) for (a) the Berea and (b) the
 774 Topopah samples; (c) Shannon entropy $H(Y_{r_i})$ versus r_i for the Topopah (circles) and the Berea
 775 (diamonds) samples; (d) bivariate normalized mutual information $I(Y_{r_i}; Y_{r_j})^* = I(Y_{r_i}; Y_{r_j}) / H(Y_{r_i})$
 776 between data at a reference support scale, Y_{r_i} , and data at larger support scales, Y_{r_j} , for $i = 1$ (blue
 777 symbols), 2 (green symbols), considering the Berea (diamonds) and the Topopah (circles) rock
 778 samples.

779



780

781 Figure 4. Information Partitioning of the multivariate mutual information, $I(Y_{r_{i+1}}, Y_{r_{i+2}}; Y_{r_i})$, considering
 782 two triplets of data and $r_i =$ (a) r_1 and (b) r_2 for the Berea sample and $r_i =$ (c) r_1 and (d) r_2 for the
 783 Topopah sample. For ease of comparison, we show the redundant, unique, and synergetic,
 784 contributions normalized by $I(Y_{r_{i+1}}, Y_{r_{i+2}}; Y_{r_i})$.

785

786